PNAS RESEARCH ARTICLE | CELL BIOLOGY

Activating STING1-dependent immune signaling in *TP53* mutant and wild-type acute myeloid leukemia

Aksinija A. Kogan[a,b], Michael J. Topper[c], Anna J. Dellomo[a,b], Lora Stojanovic[a,b], Lena J. McLaughlin[a,b], T. Michael Creed[d], Christian L. Eberly[d], Tami J. Kingsbury[a,d,e], Maria R. Baer[a,f], Michael D. Kessler[c], Stephen B. Baylin[c,g,1], and Feyruz V. Rassool[a,b,1]

Contributed by Stephen B. Baylin; received December 23, 2021; accepted April 5, 2022; reviewed by Michelle Le Beau and Sergio Rutella

DNA methyltransferase inhibitors (DNMTis) reexpress hypermethylated genes in cancers and leukemias and also activate endogenous retroviruses (ERVs), leading to interferon (IFN) signaling, in a process known as viral mimicry. In the present study we show that in the subset of acute myeloid leukemias (AMLs) with mutations in *TP53*, associated with poor prognosis, DNMTis, important drugs for treatment of AML, enable expression of ERVs and IFN and inflammasome signaling in a STING-dependent manner. We previously reported that in solid tumors poly ADP ribose polymerase inhibitors (PARPis) combined with DNMTis to induce an IFN/inflammasome response that is dependent on STING1 and is mechanistically linked to generation of a homologous recombination defect (HRD). We now show that STING1 activity is actually increased in *TP53* mutant compared with wild-type (WT) *TP53* AML. Moreover, in *TP53* mutant AML, STING1-dependent IFN/inflammatory signaling is increased by DNMTi treatment, whereas in AMLs with WT *TP53*, DNMTis alone have no effect. While combining DNMTis with PARPis increases IFN/inflammatory gene expression in WT *TP53* AML cells, signaling induced in *TP53* mutant AML is still several-fold higher. Notably, induction of HRD in both *TP53* mutant and WT AMLs follows the pattern of STING1-dependent IFN and inflammatory signaling that we have observed with drug treatments. These findings increase our understanding of the mechanisms that underlie DNMTi + PARPi treatment, and also DNMTi combinations with immune therapies, suggesting a personalized approach that statifies by *TP53* status, for use of such therapies, including potential immune activation of STING1 in AML and other cancers.

immune signaling | epigenetics | TP53 | AML | combination therapy

Significance

Our studies reveal that TP53 status in acute myeloid leukemias (AMLs) affects expression of endogenous retroviruses, PARP1, and STING1-dependent interferon signaling, leading to HRD when such cells are treated with DNA methyltransferase inhibitors (DNMTis) and poly ADP ribose polymerase inhibitors (PARPis). STING1 activity is actually increased in *TP53*-mutated AML, and STING1-dependent interferon/inflammatory signaling is further increased by DNMTi and PARPi treatment. These findings suggest that *TP53-mutated* AML may be more amenable to therapeutic strategies that further activate STING1-dependent immune responses. Thus, personalization of STING-dependent immune therapy may be an important strategy in treatment of AML and other cancers.

Acute myeloid leukemia (AML) is a genetically heterogeneous disease characterized by malignant clonal proliferation of immature myeloid cells in the bone marrow (1, 2). AML has diverse cytogenetic and molecular abnormalities that predict treatment outcomes, enable treatment stratification, and, increasingly, provide therapeutic targets (3). *TP53* alteration or loss is one of the most powerful predictors of poor outcome in AML (4–6), suggesting the need for alternative therapies. Herein, we present data with translational significance for AML involving a lesser investigated role of *TP53* as a guardian of the genome for prevention of unwanted transcription of repeat sequences (7). Furthermore, our data link this role with a similar, long-recognized guardian role for the process of DNA methylation (8).

DNA methyltransferase inhibitors (DNMTis) are approved for treatment of myelodysplastic syndromes (MDS) and are also used for treatment of AML in patients unfit for intensive chemotherapy (9, 10). The primary effect of these epigenetic agents is thought to be reversal of gene expression changes that are associated with DNA methylation abnormalities commonly found in AML. In preclinical studies, DNMTis produced more apoptosis in *TP53*-deficient than in wild-type (WT) *TP53* neoplastic fibroblasts (11, 12). These findings link to clinical data demonstrating that AML patients with *TP53* mutations had robust responses to DNMTi treatment (13). In contrast, in other studies there was no significant association between *TP53* mutations and response to treatment with DNMTis (14, 15). Although DNMTis have been widely used for the treatment of AML, and some patients have achieved durable remissions, the effects are not nearly as strong or consistent as was hoped, given the strength of preclinical data (16). Fennell et al. describe a number of possibilities for why this may be the case, including the fact that AML has historically never shown curative responses to single-agent therapy (16). Therefore, in order to increase efficacy, researchers have pursued drug treatments that can have synergistic effects with the favorable epigenetic reprogramming induced by DNMTis (17).

We have been exploring addition of Poly (ADP ribose) polymerase inhibitors (PARPis) to DNMTis (18). PARPis are approved for use in the clinic to treat BRCA-deficient or

Author contributions: A.A.K., M.J.T., L.J.M., T.J.K., M.R.B., M.D.K., S.B.B., and F.V.R. designed research; A.A.K., M.J.T., A.J.D., L.S., T.M.C., C.L.E., and M.D.K. performed research; A.A.K., M.J.T., A.J.D., and M.D.K. analyzed data; and A.A.K., M.J.T., M.R.B., M.D.K., S.B.B., and F.V.R. wrote the paper.

Reviewers: M.L.B., University of Chicago; and S.R., Nottingham Trent University.

The authors declare a competing interest. F.V.R. and S.B.B. share co-inventorship on US Provisional Patent Application No. 61/929,680 for the concept of the combinatorial therapy.

[1]To whom correspondence may be addressed. Email: frassool@som.umaryland.edu or sbaylin@jhmi.edu.

This article contains supporting information online at http://www.pnas.org/lookup/suppl/doi:10.1073/pnas.2123227119/-/DCSupplemental.

Published June 27, 2022.

homologous recombination–deficient (HRD) breast, ovarian, and prostate cancers (BC, OC, and PC) (19–21). PARPis inhibit repair of single- and double-strand DNA breaks (SSBs, DSBs) both by inhibiting PARylation and trapping PARP1/2 in DNA (22). BRCA mutations render cells deficient in homologous recombination (HR), and therefore potentially lethal DSBs formed during replication in PARP-inhibited cells cannot be repaired, leading to subsequent cell death by synthetic lethality (18, 22–25). We reported that combining PARPi with DNMTi increased PARP trapping and produced synergistic cytotoxicity in AML and triple-negative breast cancer (TNBC) cells (22). Extending these antitumor effects to nonsmall cell lung cancer (NSCLC), we also showed that DNMTis down-regulate a subset of DNA damage response genes, inducing HRD, which mimics the BRCA-mutant phenotype and sensitizes cells to PARPis (23). Similar findings were also demonstrated in our recent study in TNBC and OC (26).

DNMTis have also been shown to transcriptionally reprogram immune signaling, with significant relevance to immune therapy strategies seeking to exploit immunological modulation (17, 27–29). This reprogramming includes induction of an interferon (IFN) response via transcriptional activation of endogenous retrovirus (ERV) genes (30). These ERV genes form RNA and DNA intermediates by reverse transcription, which in turn drive immune signaling through the stimulator of interferon genes 1 (STING1) gene and other cytoplasmic double-stranded RNA (dsRNA) sensors (30–33). DNA damage induced by PARPi has been reported to activate STING1 signaling (34, 35), via cytosolic double-stranded DNA (dsDNA) (36). In our recent study in TNBC and OC, we reported a broadened response with DNMTi + PARPi combination treatment, encompassing activation of STING1-dependent IFN and inflammasome signaling leading to down-regulation of HR, thus generating an HRD phenotype in BRCA-proficient cells (26).

Herein, we define mechanistic insights linking the role of TP53 to STING1-dependent IFN signaling responses in AML. Specifically, we look at ERV gene expression levels in cells treated with DNMTis. Interestingly, we identify differential ERV gene transcriptional responses between *TP53* WT and mutant cells and stratify our mechanistic experiments on the basis of *TP53* mutation status. The rationale for this stratification is built on previous reports that TP53 plays a significant role in the maintenance of epigenetic silencing (37, 38). Mutations in *TP53*, including those causing loss of function (LOF) and dominant negative function, relieve this transcriptional repression (38). Since cytosolic dsDNA is known to drive STING1 signaling (39), and PARPis are known to increase cytosolic dsDNA (40), we also tested how PARPi treatment affects cytosolic dsDNA fragment formation and subsequent STING1 signaling. After characterizing how DNMTi + PARPi alters STING1-mediated immune signaling and HRD induction, and whether any such changes differ on the basis of *TP53* mutation status, we assay whether these effects are STING1 dependent. Thus, in the present manuscript, we bring a synthesis of events for *TP53*, STING1, DNMTis, and PARPis together in studies that are translationally relevant to AML and may be extrapolated to cancer in general.

Results

DNMTi Treatment Increases ERV Gene Expression in TP53 Mutant AML. In solid tumor models, DNMTis have previously been shown to activate STING1-mediated IFN signaling through the transcriptional activation of ERVs (26, 30, 41). Of particular interest in hematologic malignancies was a study showing strong preferential up-regulation of the ERV group 3 member 1 (*ERV3-1*) in AML patients with complex karyotypes and *TP53* mutations treated with the DNMTi decitabine (DAC) (42). Our further analysis of this Greve et al. dataset (GSE138696) (42) revealed another ERV, ERVH-3, specifically up-regulated in *TP53* mutant cells following administration of DAC (20 mg/m^2 intravenously over 1 h for 5 d) (*SI Appendix*, Fig. S1 *A* and *B*). Given these intriguing data on DAC-induced transcriptional ERV responses in *TP53* mutant AML, we determined whether these particular ERVs, as well as others identified in the Chiappinelli et al. paper (30), could be up-regulated in DNMTi-treated AML primary cells and cell lines. Given that TP53 has been shown to suppress transcription and to play a direct role in epigenetic silencing (13, 37, 43), we also hypothesized that *TP53* mutant AML cell lines would be more susceptible to DNMTi induction of viral mimicry via increased ERV transcription. We tested this hypothesis in *TP53* WT (MOLM-14, OCI-AML2, and OCI-AML3) and mutant (Kasumi-1, KG-1a, and U937) AML cell lines. Kasumi-1 cells have a gain-of-function (GOF) mutation in TP53, R248Q, while KG1a and U937 had LOF mutations in TP53. Thirteen ERVs, including ERV3-1, H-1, and previously interrogated ERVs (30), were studied by qPCR analysis following DAC treatment (10 nM, 72 h). ERV3-1 and H-1 increased twofold in *TP53* mutant vs. WT AML cell lines (*SI Appendix*, Fig. S2*A*). Importantly, ERV transcripts overall showed a two- to eightfold increase ($P < 0.005$) in all *TP53* mutant cells, irrespective of LOF or GOF mutation status, but no increase in *TP53* WT AML cell lines (Fig. 1*A* and *SI Appendix*, Fig. S2*A*; $P < 0.01$). These results were validated in the study of primary cells from AML patients (*TP53* mutant [$n = 6$], *TP53* WT [$n = 6$]) (Fig. 1*B* and Table 1 and *SI Appendix*, Fig. S2*B*). We then used the TP53 inhibitor pifithrin (500 nM, 72 h), which specifically inhibits transactivation of p53-responsive genes (44), to test whether these ERV-activating effects are directly mediated by TP53. *TP53* WT MOLM-14 AML and OCI-AML2 cells cultured with pifithrin as a single agent demonstrated significant increases in 4/13 ERVs tested (Fig. 1 *C* and *E*; $P < 0.05$). This effect was dependent on the presence of WT TP53, as treatment of the *TP53* mutant cell lines Kasumi-1 and KG1a with pifithrin did not change ERV expression (Fig. 1 *D* and *F*). Given our interest in DNMTi treatment in combination with PARPi (18, 26), we tested whether PARP inhibition with talazoparib (Tal, 5 nM, 72 h) could similarly drive ERV activation. PARPi alone did not change ERV gene expression in WT or mutant *TP53* AML cells (*SI Appendix*, Fig. S2 *C–H*), and DNMTi + PARPi drug combination treatment had similar effects on ERV gene expression as DNMTi treatment alone (*SI Appendix*, Fig. S2 *C–H*).

PARPi Drives Cytoplasmic dsDNA Increases in AML, with Effects Blunted in TP53 Mutants. Given these TP53-specific ERV findings, as well as previous reports that PARPi increases cytosolic dsDNA and drives STING1 signaling (26, 35), we compared the impact of PARPi on cytosolic dsDNA expression in *TP53* WT and mutant cell lines. Interestingly, we first found that levels of cytosolic dsDNA are increased in *TP53* WT MOLM-14 cells compared with *TP53* mutant Kasumi-1 cells (Fig. 2*A*). We first noted a distinct correlation between *TP53* mutation status and PARP1 protein expression levels, which are significantly lower in *TP53* WT cell lines (MOLM-14, OCI/AML2, and OCI/AML3) compared with *TP53* mutant cells (Kasumi-1, U937, and KG1a) (Fig. 2*A*; $P < 0.05$). Importantly, these differences in PARP1

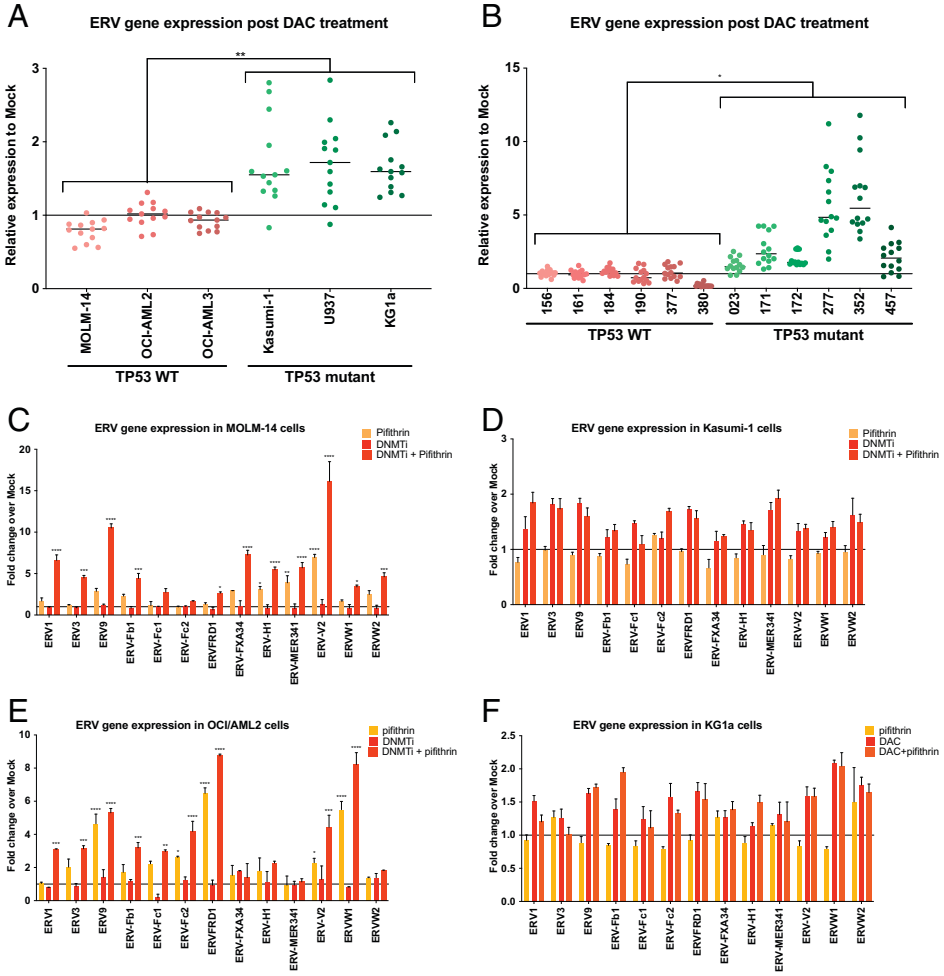

Fig. 1. DNMTi treatment increases ERV gene expression in *TP53* mutant AML. Relative RNA expression for a subset of ERV genes after mock or 10 nM DAC treatment in (*A*) *TP53* WT (MOLM-14, OCI-AML2, and OCI-AML3) and *TP53* mutant (Kasumi-1, KG-1a, and U937) cell lines (72 h, $n = 3$ biological replicates) and (*B*) *TP53* WT ($n = 6$) and *TP53* mutant ($n = 6$) primary AML PBMCs or bone marrow (BM) samples. (*C–F*) Relative RNA expression for a subset of ERV genes after mock or 10 nM DAC treatment ± 50 μM pifithrin in MOLM-14 (*C*), Kasumi-1 (*D*), OCI/AML2 (*E*), and KG1a (*F*) cells (72 h, $n = 3$ biological replicates). All data are presented as mean ± SEM, with statistical significance derived from two-tailed unpaired Student's *t* test (or ANOVA).

levels between WT vs mutant *TP53* AML seem to be universal for AML, as we observed them in primary samples from The Cancer Genome Atlas database (TCGA) (45) (Fig. 2*B*; $P = 0.002$). Treatment of AML cell lines with the PARPi Tal at a low concentration (5 nM) caused reductions in PARP1 protein levels only in WT *TP53* cell lines, and not in mutant *TP53* cells, which is consistent with these cell lines having lower levels of PARP1 at baseline (Fig. 2*C* and *SI Appendix*, Fig. S3 *A–F*). Increasing Tal concentrations (10 to 20 nM) in *TP53* mutant Kasumi-1 cells, with a high baseline level of PARP1 protein, led to a decrease in PARP1, consistent with a concentration-dependent effect on PARP1 (Fig. 2*C*). As expected, we found that levels of cytosolic dsDNA are increased in *TP53* WT MOLM-14 cells compared with *TP53* mutant Kasumi-1 cells (Fig. 2*D*). Furthermore, increasing the Tal concentration led to a concordant increase in cytoplasmic dsDNA in *TP53* mutant Kasumi-1 cells, similar to levels seen at lower concentrations in WT *TP53* cells (Fig. 2*D*).

STING1 Activity Is Increased in *TP53* Mutant AML. We found that the status of STING1 expression basally, and with our drug treatments, is crucial for the above effects. In a recent study we showed that DNMTi + PARPi treatment increases STING1 expression in TNBC and OC cells (26). To evaluate whether this mechanism explains DNMTi + PARPi efficacy in AML (18), we first characterized basal STING1 expression in primary AML TCGA samples and in AML cell lines. In TCGA, AML samples with WT *TP53* have significantly higher levels of STING1 than samples with *TP53* mutations (Fig. 3*A*; $P = 0.00021$). Western blot analysis of STING1 protein levels in AML cell lines is consistent with these data, with *TP53* WT cell lines (MOLM-14, OCI/AML2, and OCI/AML3 showing higher baseline protein levels than *TP53* mutant cell lines) (Kasumi-1, KG1a, and U937) (Fig. 3*B*). We then evaluated whether STING1 protein levels increase more significantly in *TP53* mutant cell lines after DNMTi + PARPi combination treatment. Surprisingly, we found that STING1 protein levels did not change after DNMTi, PARPi, or combination treatment in any of the cell lines tested (Fig. 3 *C* and *D* and *SI Appendix*, Fig. S4 *A–D*). We therefore considered whether STING1 protein activation (via phosphorylation) may vary with *TP53* mutation status. Indeed, while basal STING1 expression is lower in *TP53* mutants, STING1 phosphorylation, and therefore its activity, is increased at baseline in *TP53* mutant (Kasumi-1, U937, and KG1a) (Fig. 3*D* and *SI Appendix*, Fig. S4 *A* and *B*) compared to *TP53* WT (MOLM-14, OCI-AML2, and OCI-AML3) cells (Fig. 3*C* and *SI Appendix*, Fig. S4 *C* and *D*). Furthermore, in *TP53* mutant cells, phospho-STING1 protein levels increase following DNMTi treatment, but increase even further following DNMTi + PARPi combination treatment (Fig. 3 *D* and *E* and *SI Appendix*, Fig. S4 *C* and *D*). In contrast, in *TP53* WT AML cells phospho-STING1 levels are not altered by single-agent DNMTi or PARPi treatment, but increase with the drug combination (Fig. 3 *C* and *E* and *SI Appendix*, Fig. S4 *A* and *B*). These results suggest that *TP53* mutants not only have increased baseline STING1 activation,

Table 1. Cytogenetic and molecular features AML primary samples treated with DNMTi + PARPi in vitro

Sample No.	Age	Sex	WBC	% blood blasts	% marrow blasts	Karyotype	Category	Mutations	TP53 status
156	41	F	376.8	92	N/A	46,XX	Normal/ intermediate	FLT3-ITD FLT3 TKD NPM1 IDH1	WT
161	59	M	96.3	5	30	47,XY,+8	Intermediate	SRSF2 SETBP1 TET2 x 2 EZH2	WT
171	64	F	23.7	47	N/A	44–45,XX,add (1)(p36.1),-5, add (12)(p13), der(14)*t* (1, 14)(p22;p13),-16,-17,-22, +1–3mar	Complex/ unfavorable	TP53 84% TET2 IDH1	Mutant
184	51	M	80	86	85	46,XY,*t* (2, 14)(q23;q32)	Intermediate	FLT3-ITD RNX1 x 2 SF3B1	WT
190	67	M	190.6	63	N/A	46,XY,add (11)(p11.2),add (17)(p11.2)	Intermediate	SRSF2 RUNX1 TET2	WT
457	69	F	1.2	0	44	46,XX,-2[15],der(5)*t*(?2;?;5)(q23;?;q15)[15], del (7)(q21)[14],add (9)(p23)[12], del (17)(p11.2)[15],-20[4],+1–2mar	Complex/ unfavorable	TP53 42.8%	Mutant
172	67	F	37.7	55	86	45,XX,inv (3)(q21q26),-5,del (7)(q22),+mar	Complex/ unfavorable	TP53 85%	Mutant
23	61	F	56.4	70	81	42,X,der(X;17)(q10;p10),-5,der(11)add(p15)hsr (11)(q23)add (11)(q23) hsr (11)(q23),add (12)(p12),-13,add (15)(q15),add (15)(p11.2),add (19)(p13),-22,+mar[cp14]/ 42,ídem,r(11)add(15)hsr (11)(q23)add (11)(q23)hsr (11)(q23)-der (11)	Complex/ unfavorable	TP53 97%	Mutant
277	47	F	34.2	44	66	43–45,XX,+1,add (1)(q43),del (5)(q13q31),+6,-7,-16,-18,-21,der(22)ins(22:?)(q11.2;?)dup (21)(q11.2q13),+1–2mar[cp20]	Complex/ unfavorable	TP53 x2 52%, 45% NRASx2	Mutant
352	79	F	17.5	4	31	46,XX,add (2)(q36),t (3, 6)(p21;p23),-5,add (10)(p15),-11,-13,-13,-14,add (16)(q21),-17,-22,+4–8mar{cp11}	Complex/ unfavorable	TP53 78% TET2	Mutant
377	65	M	2.1	64	94	50,XY,+2,+8,der (10)(*t* (10, 12)(p12;q13),del (11)(q13q23),+19,+21	Complex/ unfavorable	KIT	WT
380	38	F	100	80	56	46,XX	Normal/ intermediate	NRAS DNMT3A NPM1 PTPN11 FLT3 IDH2	WT

but also have the capacity to further increase STING1 activity compared with WT *TP53* AML cells.

DNMTi Treatment Increases IFN and TNFa/NF-κB Inflammasome Signaling in *TP53* Mutant AML. Given this increased STING1 activity in AML, and our previous reports that DNMTi + PARPi combination treatment induced STING1 and IFN signaling in TNBC and OC (26), we next examined whether DNMTi and/or PARPi combination treatment also drives immune signaling in *TP53* mutant AML, a poor-risk subtype. Hallmarks and Kyoto Encyclopedia of Genes and Genomes (KEGG) pathway analysis of genome-wide expression data from WT *TP53* MOLM-14 cells supported the transcriptional activation of multiple immune response pathways, including *IFNs*, *TNFa*, and the inflammatory response, by DNMTi + PARPi combination treatment, whereas single-agent DAC or Tal treatment produced a markedly less robust response (Fig. 4*A* and *SI Appendix*, Fig. S5). To validate these data, we performed qPCR analysis of a panel of immune genes, including *IFNs*, *TNFa*, and inflammasome genes, that we selected based on our genome-wide expression data, as well as previous data from our laboratories (26) (Fig. 4*B*). In MOLM-14 cells, DNMTi treatment alone led to modest increases in expression in only 3 of the 24 immune genes tested (*EGR1*, *IFI44*, and *IL7R*) (Fig. 4*B* and *SI Appendix*, Fig. S6*A*; $P < 0.05$). In contrast, DNMTi + PARPi combination treatment significantly increased expression of 13 of these tested genes (*B2M*, *EGR1*, *GADD45*, *ID2*, *IFI16*, *IFI30*, *IFNb*, *IL7R*, *IRF3*, *IRF7*, *IRF9*, *TBK1*, and *STING11*) (Fig. 4*B* and *SI Appendix*, Fig. S6*A*; $P < 0.01$). Investigation of two additional *TP53* WT AML cell lines (OCI-AML2 and OCI-AML3) revealed similar gene expression changes (*SI Appendix*, Fig. S6 *B* and *C*). The pattern of IFN gene expression is quite different in *TP53* mutant Kasumi-1 cells, as DNMTi

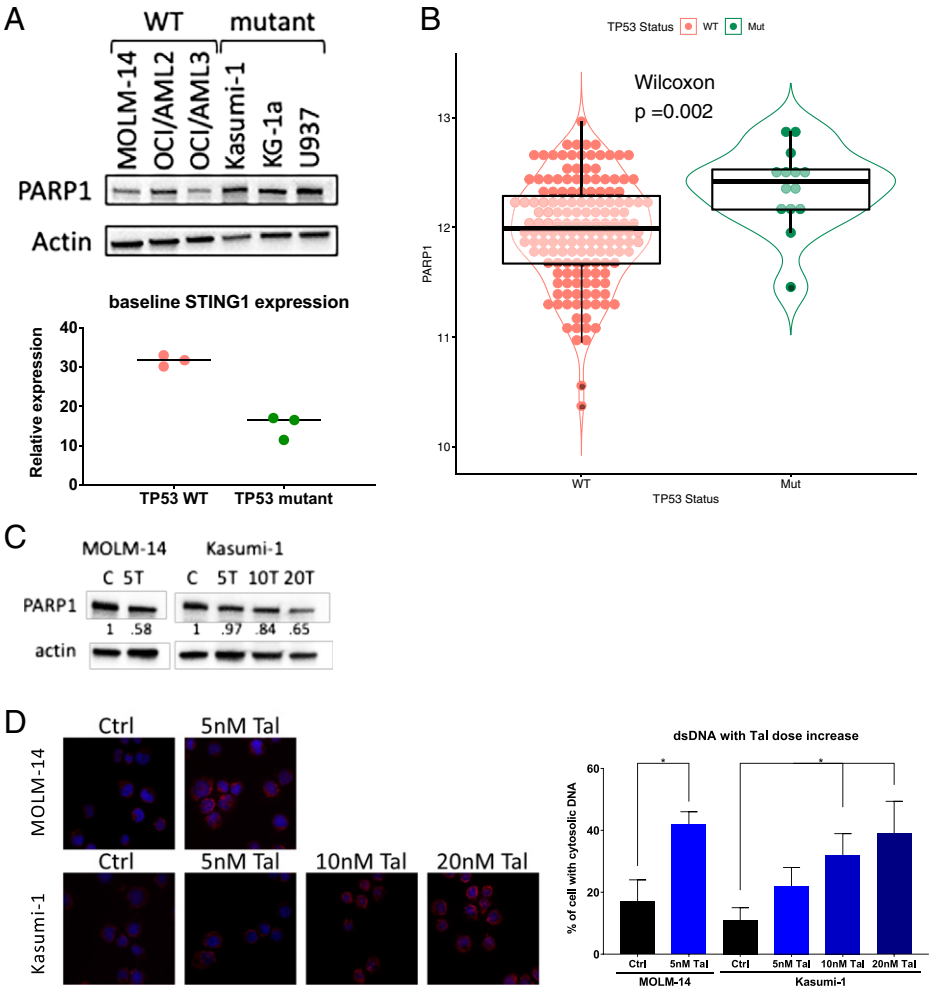

Fig. 2. PARPi treatment increases cytosolic dsDNA in *TP53* mutant AML in a dose-dependent manner. (*A*) Immunoblot for PARP1 in *TP53* WT (MOLM-14, OCI/AML2, and OCI/AML3) and *TP53* mutant (Kasumi-1, KG-1a, and U937) cell lines at baseline with β-actin used as a loading control ($n = 3$ biological replicates). (*B*) Violin plots for PARP1 mRNA expression in TCGA AML samples grouped by *TP53* status. (*C*) Immunoblot for PARP1 after mock, or 5 nM, 10 nM, and 20 nM Tal treatment in MOLM-14, and Kasumi-1 cell lines with β-actin used as a loading control (72 h, $n = 3$ biological replicates). (*D*) Representative immunofluorescence images for dsDNA (left) and quantified (right) in MOLM-14 and Kasumi-1 cells after mock, or 5 nM, 10 nM, and 20 nM Tal treatment (72 h, $n = 3$ biological replicates). All data are presented as mean ± SEM, with statistical significance derived from two-tailed unpaired Student's *t* test (or ANOVA), or Wilcoxon signed-rank test.

treatment alone drives pronounced increases in expression of 7/24 *IFN* genes (*ID2*, *IFI27*, *IFI44*, *IL7R*, *IRF9*, *OASL*, and *SERPINB8*) and DNMTi + PARPi combination treatment increases the magnitude of *IFN*-related gene expression even further (Fig. 4*B* and *SI Appendix*, Fig. S6*D*; $P < 0.05$). Investigation of additional mutant *TP53* AML cell lines (KG-1a and U937) revealed a similar pattern of *IFN* gene expression differences (*SI Appendix*, Fig. S6 *E* and *F*). Importantly, these results were replicated in AML primary samples (*TP53* mutant [$n = 6$] and *TP53* WT [$n = 6$]) (Table 1 and Fig. 4 *C* and *D* and *SI Appendix*, Fig. S7 *A–L*).

DNMTi Treatment Drives Decreases in HR in *TP53* Mutant AML. In our previous publications we have shown that DNMTi + PARPi combination treatment leads to increased DNA damage and reduced HR capacity (18, 23), and we most recently connected this HRD to immune signaling in solid tumors (26). To examine the connection between immune signaling and HR in AML, we used the STRING database and computational tool (46) to perform network analysis for known protein interactions between targets of interest. This analysis revealed TP53 as a potential basal central node intersection for genes in the *IFN* pathway and DNA damage genes, including HR-related factors (Fig. 5*A* and *SI Appendix*, Fig. S8*A* [expanded view]). In support of this predicted protein network interaction, treatment of *TP53* WT MOLM-14 cells with *IFNβ* or TNFα/IL-1β showed increases in downstream *IFN* gene expression levels, and simultaneously, decreases in DNA repair gene expression (*SI Appendix*, Fig. S8 *B* and *C*). Accordingly, these treatments down-regulate HR activity as measured via an in vitro plasmid reporter assay (23, 26) (Fig. 5*B* and *SI Appendix*, Fig. S8*D*). In further validation of the predicted direct relationship between IFN signaling and HR activity, treatment of MOLM-14 AML cells with the JAK inhibitor ruxolitinib (Rux), which inhibits IFN pathway signaling (47), rescues HR activity (Fig. 5*B*).

Given the above central role of TP53 in the interactions under study, we hypothesized that expression and activity of HR-related genes following DNMTi and/or PARPi treatment would differ between *TP53* WT and mutant AML cell lines. Indeed, while DNMTi or PARPi treatment alone had no significant effect on HR gene expression in *TP53* WT MOLM-14 cells (Fig. 5*C*; $P < 0.0001$ and *SI Appendix*, Fig. S9*A*), DNMTi treatment resulted in a decrease in expression of HR-related genes in *TP53* mutant Kasumi cells, and the DNMTi + PARPi combination treatment further decreased expression of these genes (Fig. 5*C*; $P < 0.001$ and *SI Appendix*, Fig. S9*D*). Importantly, treatment of additional AML cell lines (*SI Appendix*, Fig. S9 *B*, *C*, *E*, and *F*) and *T53* WT ($n = 6$) and mutant ($n = 6$) primary samples (Fig. 5 *E* and *F* and *SI Appendix*, Fig. S10 *A–L*) with DNMTi, PARPi, and DNMTi + PARPi combined produced similar HR gene expression patterns and effects on HR activity as shown above (Fig. 5*D*).

STING1 Inhibition Abrogates IFN Signaling and Rescues HR Activity in TP53 WT and TP53 Mutant AML. We next found that a direct connection between IFN signaling and HR activity

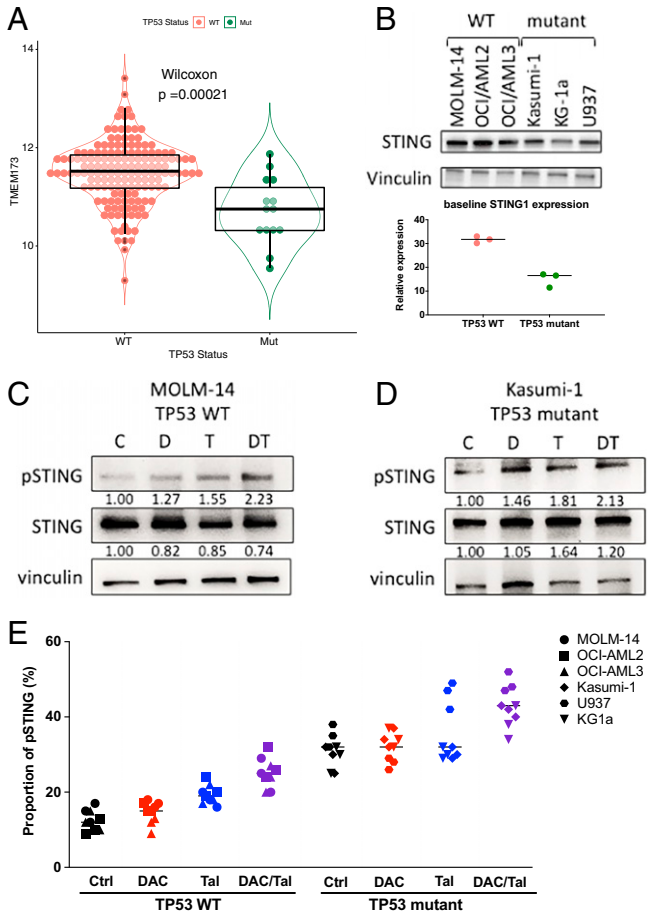

Fig. 3. STING1 activity is increased in TP53 mutant AML. (*A*) Violin plots for STING1 mRNA expression in TCGA AML samples grouped by TP53 status. (*B*) Immunoblot for STING1 in TP53 WT (MOLM-14, OCI/AML2, and OCI/AML3) and TP53 mutant (Kasumi-1, KG-1a, and U937) cell lines at baseline with vinculin used as a loading control ($n = 3$ biological replicates). (*C* and *D*) Immunoblot for pSTING1 and STING1 in MOLM-14 (*C*) and Kasumi-1 (*D*) cells after mock, 10 nM DAC, 5 nM Tal, or DAC/Tal combination: 10 nM DAC + 5 nM Tal treatment with vinculin used as a loading control, quantified values below each respective protein (72 h, $n = 3$ biological replicates). (*E*) Quantification of proportion of pSTING1 in MOLM-14, OCI/AML2, OCI/AML3, Kasumi-1, U937, and KG1a cells after mock, 10 nM DAC, 5 nM Tal, or DAC/Tal combination: 10 nM DAC + 5 nM Tal treatment (72 h, $n = 3$ biological replicates). All data are presented as mean ± SEM, with statistical significance derived from two-tailed unpaired Student's *t* test (or ANOVA), or Wilcoxon signed-rank test.

in AML cells treated with DNMTi and/or PARPi is STING1 dependent. We used H-151, which is a highly potent covalent antagonistic inhibitor of STING1 (48). The increases in *IFN* gene expression seen with DNMTi + PARPi combination treatment in *TP53* WT MOLM-14 cells were significantly decreased with the addition of H-151 (Fig. 6*A*; 500 nM, $P < 0.001$ and *SI Appendix*, Fig. S11*A*). Similarly, in *TP53* mutant Kasumi-1 cells, H-151 treatment significantly decreased the altered *IFN* gene expression seen in cells treated with either DNMTi ($P < 0.05$) or DNMTi + PARPi combination ($P < 0.0001$) (Fig. 6*A* and *SI Appendix*, Fig. S11*B*). With respect to effects of STING1 inhibition on HR gene expression, in WT *TP53* MOLM-14 cells, H-151 treatment rescued the decreased expression of HR genes that is driven by DNMTi + PARPi combination treatment (Fig. 6*B*; $P < 0.001$ and *SI Appendix*, Fig. S11*C*). Notably, H-151 cotreatment also resulted in robust rescue of HR gene expression in *TP53* mutant Kasumi-1 cells treated with DNMTi or with DNMTi + PARPi (Fig. 6*B*; $P < 0.0001$ and *SI Appendix*, Fig. S11*D*). H-151 also rescued the DNMTi + PARPi combination treatment–induced reduction in HR activity in WT *TP53* MOLM-14 cells (Fig. 6*C*; $P < 0.001$) as well as in *TP53* mutant Kasumi-1 cells (Fig. 6*D*; $P < 0.0001$), further supporting the mechanistic role of STING1 in HRD induction. We further confirmed these findings in C1498 AML mouse cells with WT *TP53* (49, 50) using H-151 as well as *STING1* knockout (KO) cells generated with CRISPR-CAS9 (Fig. 6 *E* and *F* and *SI Appendix*, Fig. S12 *A*–*C*). Finally, we compared isogenic mouse AML C1498 cells with *TP53* WT and KO (*SI Appendix*, Fig. S12*D*) for some of the gene expression changes described above. First, *TP53* KO cells (clone Sg1) were significantly sensitive to growth inhibition by DAC (*SI Appendix*, Fig. S12*E*). Second, mERVL, previously shown to be up-regulated with DNMTi treatment in mouse ovarian cancer cells (51) and IRF7, showed significant ($P < 0.05$) increases in expression only in the *TP53* KO following DAC treatment (*SI Appendix*, Fig. S12*F*; $P < 0.05$).

DNMTi Treatment In Vivo Increases Inflammasome Signaling, Validating In Vitro Data. For in vivo validation of the effects of our drugs on inflammatory and inflammasome signaling, we used the Greve et al. (42) datasets (GSE138696) of both mutant ($n = 6$) and WT *TP53* ($n = 7$) AML patient samples (13 pretreatment and 13 posttreatment samples) treated with DAC (20 mg/m2 intravenously over 1 h daily for 5 d) in the DECIDER trial (NCT00867672). As a proof of concept, we first evaluated whether *TP53* mutational status impacted the presentation of the overall transcriptome by principal component analysis (PCA). These data demonstrated transcriptome-based clustering of samples driven by *TP53* mutation status in a manner that exceeds treatment-induced effects (*SI Appendix*, Fig. S13*A*). Next, we sought to elucidate whether there would be a differential transcriptional response to DAC depending on *TP53* mutation status. A total of 58 differentially expressed genes (21 up-regulated and 37 down-regulated) (*SI Appendix*, Fig. S13*B*) were found and 19 of 50 Hallmarks pathways were significantly differentially enriched (false discovery rate [FDR] adjusted [adj] *P* value <0.05) (Fig. 7 *A* and *B*). As a validation of our in vitro findings, we observed significant up-regulation of inflammation-associated gene sets, TNFA signaling via NF-κB, and IL-2/STAT5 signaling, in *TP53* mutant samples following DAC treatment (Fig. 7 *A* and *B*). Given the pronounced differential clustering provided by PCA in *SI Appendix*, Fig. S13*A*, we next defined to what extent the pretreatment transcriptional signature might be distinct in *TP53* mutant vs. WT samples. Differential expression analysis revealed a total of 850 genes (439 up-regulated and 411 down-regulated, which were significantly different in *TP53* mutant relative to WT patient samples (*SI Appendix*, Fig. S13*C*). While gene level differences between *TP53* mutant and WT were profound in the basal setting, pathway evaluation of these data were far less striking, with only 4 of 50 pathways emerging in this analysis (FDR adjusted *P* value 0.14) (Fig. 7 *C* and *D*). Expanding our assessment of inflammation-associated gene signatures, we assayed the gene level presentation of the Hallmarks *TNFA NF-κB* pathway by unsupervised hierarchical clustering, About half of the genes contained in this pathway were distinct in *TP53* mutant and WT in the basal setting, while the remaining half were modified by DAC and differentially responsive depending on *TP53* status (Fig. 7*E*). The basal sample presentation of the genes contained in this pathway is worth special mention, as the balance of relative positive and negative Z scores discovered between *TP53* mutant and WT samples might explain the lack of pathway enrichment noted, and in this setting is more suggestive of

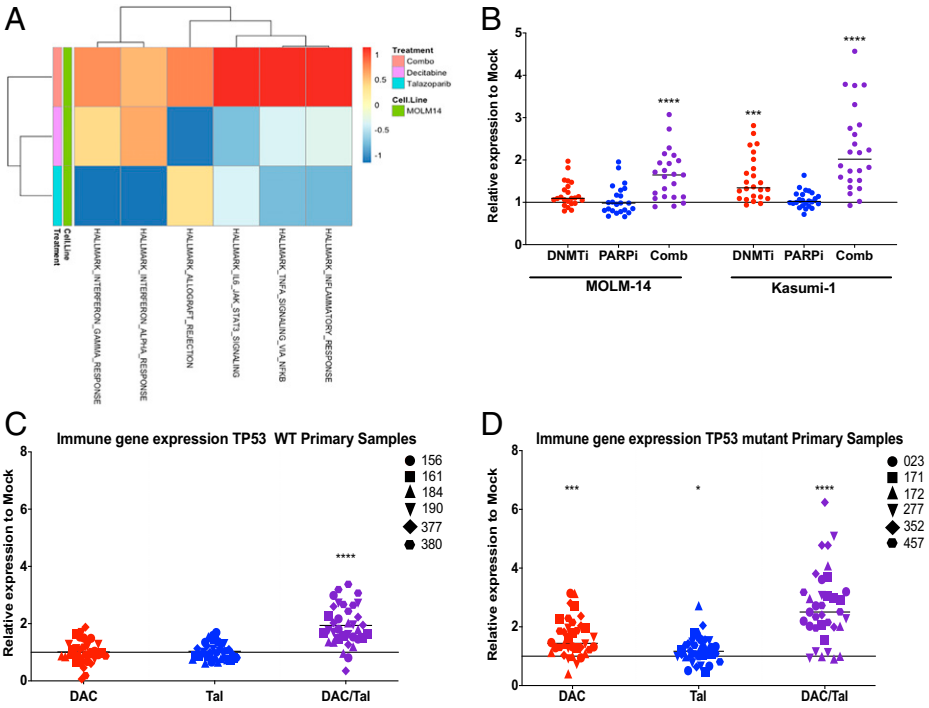

Fig. 4. DNMTi treatment increases IFN signaling in TP53 mutant AML. (*A*) Unsupervised hierarchical clustering of MSigDB Hallmarks pathways normalized enrichment scores for MOLM-14 after 10 nM DAC, 5 nM Tal, or DAC/Tal combination: 10 nM DAC + 5 nM Tal treatment, cDNA microarray data. Blue: down-regulated Hallmark pathways, red: up-regulated Hallmark pathways, pathway ranking metric: Log2 fold change relative to mock (72 h). (*B*) Relative RNA expression for a subset of immune genes after mock, 10 nM DAC, 5 nM Tal, or DAC/Tal combination: 10 nM DAC + 5 nM Tal treatment in *TP53* WT MOLM-14 and *TP53* mutant Kasumi-1 AML cell lines (72 h, $n = 3$ biological replicates). (*C* and *D*) Relative RNA expression for a subset of immune genes after mock, 10 nM DAC, 5 nM Tal, or DAC/Tal combination: 10 nM DAC + 5 nM Tal treatment in TP53 WT (*C*) and mutant (*D*) AML primary samples (72 h, $n = 3$ biological replicates). All data are presented as mean ± SEM, with statistical significance derived from two-tailed unpaired Student's *t* test (or ANOVA).

specific genes being the defining characteristics, rather than entire pathways being on versus off.

An important remaining question is whether our above results for a subset of DECIDER trial patients track with the efficacy of DAC treatment in AML. While the full clinical results of this trial remain to be compiled, early clinical results reported in recent post hoc analyses for a small number of patients in the DECIDER trial does show the efficacy of DAC treatment tracking with *TP53* mutation status (52). This suggests that our results above in Fig. 7 may well track with *TP53* mutation status and treatment efficacy and the full analyses forthcoming will be awaited to substantiate this.

Discussion

In this mechanistic study, we show that DNMTis drive activation of ERVs and STING1-dependent IFN and TNFa signaling in AML in a TP53-dependent fashion. Notably, enhanced ERV activation is linked to the presence of mutant versus WT *TP53* in AML cell lines and patient samples. A similar pattern was seen for IFN and TNFa signaling, which is consistent with previous studies that have shown STING1 activation via ERV transcript–generated dsRNA (30, 53). Our findings provide translationally relevant insights into the importance of the presence of widespread TP53 binding sites near genomic repeat elements and a suggested guardian role promoting the silencing of such elements in the genome (54). The findings bring a therapy paradigm into juxtaposition with previous suggestions that mutation or abrogation of *TP53* in cancer cells may impact how DNMTis transcriptionally relieve the silencing of repeat elements present in normal somatic cells (38, 54–56). Our data would appear to suggest that this affects both GOF and LOF TP53 mutations, since both mutation types would alter the DNA binding domain and abrogate its binding to TP53 response elements (REs) (6). Moreover, our direct link between TP53 and DNMTis demonstrates why *TP53* mutant AML cells may be significantly more sensitive, and poised to be immunologically reactive, to DNMTi treatment. This has potential implications for the treatment of AML and suggests approaches for strategically activating immune signaling in *TP53* mutant AML. This is of particular importance because *TP53* alteration or loss is one of the most powerful predictors of poor treatment outcomes in AML (4–6) (schematic model, Fig. 7*F*). Moreover, AMLs with *TP53* alterations fare less well even when DNMTis are combined with venetoclax, shown to increase responses in AML (57).This suggests novel DNMTi therapy combinations are needed.

In addition to relevance of our data to DNMTis, our present findings have implications for PARPi induction of synthetic lethality in BRCA-WT TNBC and OC cells (19, 58). This paradigm is also dependent upon activation of IFN signaling by increased cytosolic dsDNA levels (26, 40, 59). PARPi treatment also increased cytosolic dsDNA in *TP53* WT AML cells, but this mechanism is minimally operative for immune signaling in *TP53* mutant AML cells. One possible explanation for this is that PARP1 levels were significantly increased in *TP53* mutant samples, and so higher PARPi concentrations are required to disrupt PARP1 activity. Indeed, others have reported elevated PARP1 levels in many therapy-resistant cancers, which is understood to reflect increased selective pressure toward DNA repair activity and genome instability (60–63). All of these findings suggest that PARP expression levels may be useful as a biomarker of both PARPi efficacy and potential response to immune therapies.

The role of STING1 activation in our findings bears special mention as a critical factor for activating anticancer immune responses not only in AML, but in cancer in general. Notably, STING1 expression is reduced in many tumors, and researchers are actively pursuing ways of driving STING1-dependent immune signaling (64–67). In accordance with TCGA data, our studies show that AML cells with *TP53* mutations have reduced STING1 gene expression compared with *TP53*-WT AML cells. STING 1 is localized to chromosome 5q and deletions [del(5q)] in our AML patients with mutant *TP53* would lead to deletion of STING1 and haploinsufficiency. After recently reporting that DNMTi treatment can

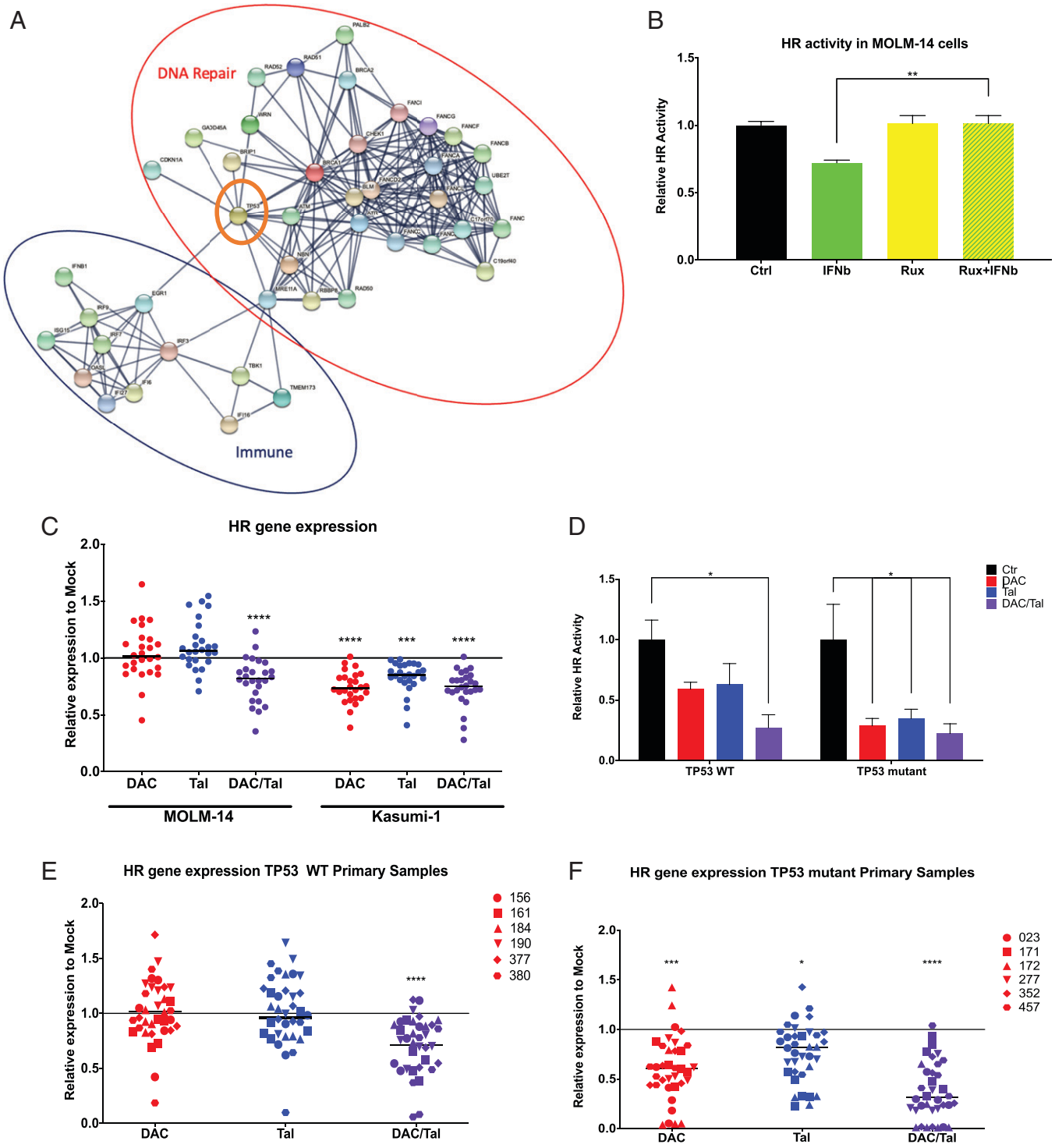

Fig. 5. DNMTi treatment drives decreases in HR in TP53 mutant AML. (*A*) STRING protein–protein interaction map of homologous recombination and IFN genes of interest. See *SI Appendix*, Fig. S5*A* for an expanded version, overlayed ellipses annotate immune (blue), DNA repair (red) clusters, and TP53 (orange). (*B*) Relative HR activity analysis 24 h after 5 μM ruxolitinib, 100 ng/mL IFNβ, or 5 μM ruxolitinib + 100 ng/mL IFNβ treatment in MOLM-14 cells ($n = 3$ biological replicates). (*C*) Relative RNA expression for a subset of HR genes after mock, 10 nM DAC, 5 nM Tal, or DAC/Tal combination: 10 nM DAC + 5 nM Tal treatment in *TP53* WT MOLM-14 and *TP53* mutant Kasumi-1 cell lines (72 h, $n = 3$ biological replicates). (*D*) Relative HR activity analysis in MOLM-14 and Kasumi-1 cell lines after mock, 10 nM DAC, 5 nM Tal, or DAC/Tal combination: 10 nM DAC + 5 nM Tal treatment (72 h, $n = 3$ biological replicates). (*E* and *F*) Relative RNA expression for a subset of HR genes after mock, 10 nM DAC, 5 nM Tal, or DAC/Tal combination: 10 nM DAC + 5 nM Tal treatment in TP53 WT (*E*) and mutant (*F*) AML primary samples (72 h, $n = 3$ biological replicates). All data are presented as mean ± SEM, with statistical significance derived from two-tailed unpaired Student's *t* test (or ANOVA).

transcriptionally activate STING1 in TNBC and OC (26), we now show that AML cells with *TP53* mutations have higher STING1 activity at baseline, and that it increases even further following DNMTi and PARPi treatment. While we do not yet understand the underlying mechanism for the increase in phosphorylated STING1 and STING1 activity in *TP53* mutant cells, we believe that it may at least in part be explained by how increased PARP1 expression in our data and TCGA can affect the "noncanonical" STING1 pathway (68). In accordance with this data, TCGA analysis of other targets, including IFI16,

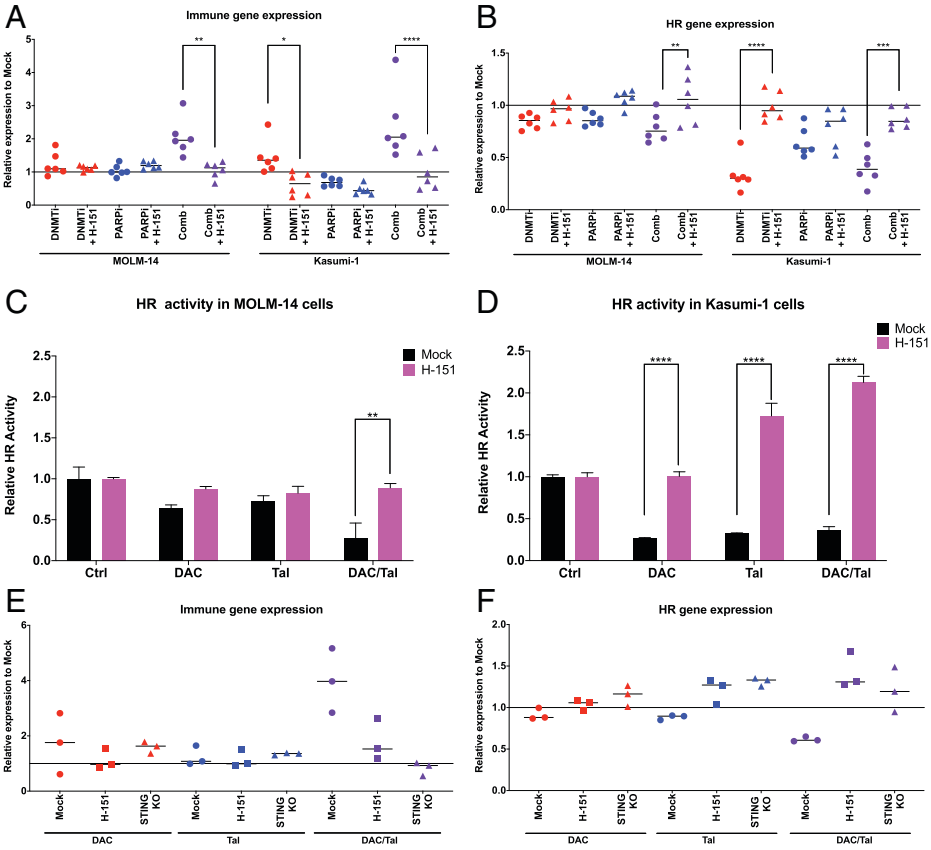

Fig. 6. STING1 inhibition abrogates IFN signaling and rescues HR activity in TP53 WT and TP53 mutant AML. (*A*) Relative RNA expression for a subset of immune genes after mock, 10 nM DAC, 5 nM Tal, or DAC/Tal combination: 10 nM DAC + 5 nM Tal treatment ± 500 nM STING1i (H-151) for all conditions in MOLM-14 and Kasumi-1 AML cell lines (72 h, $n = 3$ biological replicates). (*B*) Relative RNA expression for a subset of HR genes after mock, 10 nM DAC, 5 nM Tal, or DAC/Tal combination: 10 nM DAC + 5 nM Tal treatment ± 500 nM STING1i for all conditions in MOLM-14 and Kasumi-1 cell lines (72 h, $n = 3$ biological replicates). (*C* and *D*) Relative HR activity analysis of MOLM-14 (*C*) and Kasumi-1 (*D*) cells after 72-h treatment with mock, 10 nM DAC, 5 nM Tal, or DAC/Tal combination: 10 nM DAC + 5 nM Tal ± 500 nM STING1i for all conditions ($n = 3$ biological replicates). (*E* and *F*) Relative expression of immune (*E*) and HR (*F*) genes after CRISPR KO of STING1 or cotreatment with 500 nM STING1i in C1498 mouse AML cells treated with mock, 10 nM DAC, 5 nM Tal, or DAC/Tal combination: 10 nM DAC + 5 nM Tal ± 500 nM STING1i for all conditions (72 h, $n = 3$ biological replicates). All data are presented as mean ± SEM, with statistical significance derived from two-tailed unpaired Student's *t* test (or ANOVA).

ATM, and well as TRAF6, show up-regulation in *TP53* mutant AML cells and may explain increased STING1 activity via the noncanonical pathway. Moreover, while STING1 activity in *TP53* WT AML models increases after DNMTi + PARPi combination therapy, these increases are more modest than those seen in AML cells with *TP53* mutations. Therefore, while induction of IFN signaling and HRD in both *TP53* mutant and WT cells is STING1 dependent, *TP53* mutant AMLs seem to be particularly amenable to STING1 activation via epigenetic reprogramming and may be good candidates for other STING1 pathway activation strategies.

Overall, our work has implications for therapy strategies reliant on activating innate immune pathways. Trials of other immune therapies in AML, including those based on PD-1 or CTLA-4 inhibition, have yielded modest clinical efficacy (69), underscoring the need to enhance these therapies with other agents, as well as to focus on AML subgroups such as those with *TP53* mutations and complex karyotypes that may already be primed to respond to immunotherapy. Our data suggest that AML cells with *TP53* abnormalities have increased STING1 activation. A recent report by Vadakekolathu et al. reported that IFN-gamma signaling is increased in *TP53* mutant AML and that this AML subgroup exhibits immune infiltration and responds to flotetuzumab immunotherapy (70). Additionally, our analysis of transcriptome data from an AML clinical trial shows a distinct genotype driven transcriptome state both at baseline and in response to DAC, wherein patients with *TP53* mutations demonstrate both a heightened activation of interferon-gamma signaling basally and further mobilization of inflammatory pathways in response to DAC. Thus, AML patients with *TP53* mutations might present with a differential tumor-immune microenvironment relative to those with WT *TP53* (52). In solid tumors, DNMTi treatment has also been shown to increase the expression of immune checkpoint molecules such as PD-L1 and CTLA-4, which may represent additional synergistic potential (71–74). In fact, recent reports describe encouraging preliminary results in which DNMTi + anti–CTLA-4 combination therapy leads to decreased tumor burden and improved survival in melanoma and OC mouse models (30, 74, 75). Additional clinical and preclinical research will increase our understanding of immune responses in *TP53* mutant AML and will further enable increasingly effective combination treatments. Given the current limited ability to predict immunooncological treatment response, our findings hold particular promise with regard to identification of a specific molecular target with sensitivity to immune-modulatory treatment (76). Finally, *TP53* mutations have a consistent pattern of mutations/cytogenetic abnormalities, and the transcriptional profile will likely reflect not only TP53 status, but the collective molecular profile. Our findings may extend to other cancers with *TP53* mutations and may support the use of epigenetic treatments in a wider range of malignancies.

Methods

Cell Culture. Human AML cell lines were cultured as described in *SI Appendix, Supplemental Methods*. Primary AML patient samples were obtained following informed consent on a protocol approved by the institutional review board (IRB) of the University of Maryland School of Medicine (IRB H25314). Mononuclear cells (MNCs) from AML primary samples were isolated by density centrifugation over Ficoll-Paque (Sigma-Aldrich) and were cultured in iscove modified dulbecco media (IMDM) with 20% fetal bovine serum (FBS), without cytokine supplementation in 37 °C incubators with 5% CO_2.

Drug Treatments In Vitro. The DNTMi DAC (Sigma-Aldrich) was prepared as a stock solution of 10 mM in dimethyl sulphoxide (DMSO) and stored at −80 °C in single-use vials. Cell lines were treated daily with 10 nM DAC. The PARPi Tal

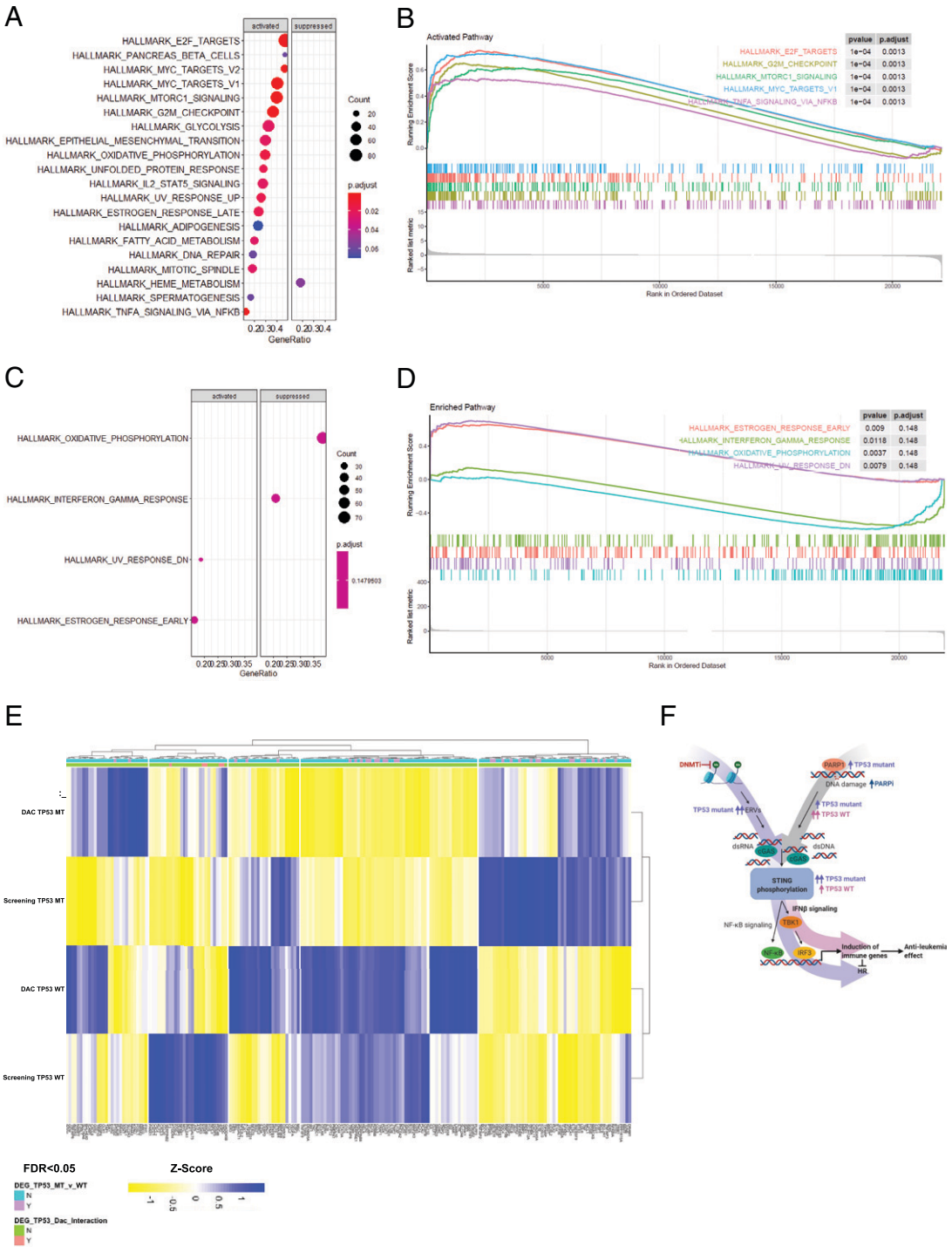

Fig. 7. Induction of inflammasome related signaling by decitabine in TP53 mutant AML patients. (*A* and *B*) Gene set enrichment analysis (GSEA) of Hallmarks pathway for TP53 status (mutant ([MT] vs. WT) and treatment (Dac vs. screening) interaction analysis of GSE138696 dataset. Pathway dot plot, color indicates adjusted *P* value, and size indicates gene count (*A*). Normalized enrichment score plot for top five activated Hallmarks pathways (*B*). (*C* and *D*) GSEA of Hallmarks pathway for TP53 status (MT vs. WT) in screening samples of GSE138696 dataset. Pathway dot plot, color indicates adjusted *P* value, and size indicates gene count. (*C*) Normalized enrichment score plot for top five enriched Hallmarks pathways. (*D*) For each group biological replicate *n* values are as follows: Dac_WT *n* = 7, screening_WT *n* = 7, Dac_MT *n* = 6, screening MT *n* = 6, WT, wild-type TP53; MT, mutant TP53. (*E*) Heatmap of Hallmarks TNF_NFKB pathway from MSigDB. Unsupervised hierarchical clustering of Z score scaled average log2 intensity values by Ward's method. Blue indicates positive Z score; yellow indicates negative Z score. Differentially expressed genes (DEG) tracks associated with heatmap are derived from differential expression analysis of screening samples for the following comparisons: MT vs. WT and TP53 Dac interaction. Genes are scored as yes or no for differential expression based on FDR adjusted *P* value <0.05. (*F*) Diagrammatic representation of therapeutic molecular model of DNMTi DAC and/or PARPi TAL treatment impacted by TP53 mutant status in AML. Left arrow or route depicts effects of DAC treatment, which significantly increases expression of ERV transcripts that lead to cytosolic dsRNA in TP53-mutated vs. WT cells. *Right* arrow or route depicts effects of PARPi treatment, which induces cytosolic dsDNA. The target of PARPi, PARP1 is actually increased in *TP53* mutant cells. Therefore, at given concentrations of PARPi TAL, increased cytosolic dsDNA is seen in TP53-WT vs. TP53-mutated cells. Both *Left* and *Right* arrows or routes converge on STING1, the key mediator of interferon and inflammasome signaling. STING1 is activated by posttranslational phosphorylation, and at baseline phospho-STING1 is increased in TP53 mutant vs. WT cells, potentially through noncanonical STING1 signaling pathways. Treatment with DAC and/or TAL can further increase STING1 activity. In TP53-mutated cells, downstream interferon and inflammasome signaling is driven by DAC treatment and further increased by DAC/TAL combination treatment. In contrast, in TP53-WT cells increased by interferon and inflammasome signaling is seen only with the DAC/TAL combination treatment. Increased interferon and inflammasome signaling leads to HRD and antileukemia effects.

(Pfizer) was prepared as a stock solution of 5 mM in DMSO and stored at −80 °C. Cell lines were treated with 5 nM Tal every 72 h. For combination treatments, cells were treated with 10 nM DAC and 5 nM Tal on day 1, and DAC was added to cells at the appropriate concentration on days 2 and 3 for a final concentration of 10 nM. Cells were harvested after 72 h. Additional information relevant to drug treatments is provided in *SI Appendix, Supplemental Methods*.

RNA Extraction and Quantitative PCR. Total RNA was isolated from cultured cells using the NucleoSpin RNA Plus kit (Macherey-Nagel). cDNA was synthesized by converting 1 to 2 μg of RNA using High Capacity cDNA Reverse Transcription kits (Applied Biosystems). qRT-PCR was performed using Power Sybr Green PCR Master Mix (Applied Biosystems) in a CFX384 Touch Real-Time PCR system (Bio-Rad). The sequences of primers used are listed in *SI Appendix*.

Immunofluorescence Staining. Detailed information relevant to immunofluorescence staining is provided in *SI Appendix, Supplemental Methods*. Images were examined and acquired using an Eclipse 80i Nikon fluorescent microscope (100×/1.4 oil). Images were captured using a charge-coupled device (CCD) camera and NIS Elements imaging software (BR 3.00, Nikon).

TCGA Analysis. To evaluate STING1 gene expression values (labeled "TMEM173" in processed TCGA legacy data) between samples with and without *TP53* mutations, we used the TCGAbioinks R package (77) to leverage transriptomics data from The Cancer Genome Atlas (45). Using samples from the "TCGA-LAML" TCGA leukemia cohort, we quantified and compared normalized expression values from legacy data (i.e., hg19) derived from RNA-sequencing (RNA-seq) experiments. For this comparative analysis, we defined 16 samples as *TP53* mutation carriers (*SI Appendix*, Table S2) using *TP53* mutation carrier status data from Vadakekolathu et al. (78). We used The Wilcoxon rank sum test as implemented in the stat_compare_means function of the ggpubr package to evaluate the statistical significance of log-transformed STING1 gene expression distributional differences.

Protein Extraction and Immunoblotting. Detailed information relevant to protein extraction and immunoblotting is provided in *SI Appendix, Supplemental Methods*. Antibodies used were PARP1 rabbit monoclonal (1:1,000, Cell Signaling), anti–β-actin mouse monoclonal (1:10,000), pSTING1 (TMEM173) rabbit monoclonal (1:1,000, Cell Signaling), STING1 (TMEM173) rabbit monoclonal (1:1,000, Cell Signaling), and vinculin rabbit monoclonal (1:1,000, Cell Signaling).

Microarray Sample Preparation and Analysis. Total RNA was isolated using the NucleoSpin RNA extraction kit. RNA was quantified with NanoDrop ND-1000 followed by quality assessment with 2100 Bioanalyzer (Agilent Technologies). Microarray sample labeling, hybridization, and data extraction were performed as previously described (26).

Pathway Analysis of Microarray Data. Microarray derived log2 fold change values were preranked prior to running fgsea (79) using Hallmarks pathways as contained in MSigDB (80). Resulting normalized enrichment scores were read into the pheatmap package (81), Z-score transformed, and then clustered using Ward.D2.

STRING Protein–Protein Interaction Map. Homologous recombination and interferon genes of interest were used as input for exploratory analysis using string-db (46), a computational resource, which summarizes known and predicted protein–protein interactions culled from experimental data from several databases: DIP, BioGRID, HPRD, IntACT, MINT, and PRB and curated data from Biocarta, Biocyc, GO, KEGG, and Reactome. The comparisons selected for input were specific for homo sapiens and included all genes used for qRT-PCR analysis. Interaction scores are assigned based on probabilities derived from various evidence channels and normalized for random associations previously described (82). For the specific plot rendered, only high confidence interactions (0.900) are depicted.

HR Repair Analysis. HR repair analysis was performed as previously described (23).

CRISPR-Engineered Cell Lines. STING1 sgRNA targeting exon 3 was expressed from lentiCRISPR v2 [Addgene plasmid No. 52961 (http://n2t.net/addgene:52961)] to generate C-1489 STING1 KO cells. Detailed information relevant to CRISPR-engineered cell lines is provided in *SI Appendix, Supplemental Methods*.

Statistical Analysis. Unless otherwise defined, all data are presented as mean ± SEM. Statistical analysis for biological assays and mouse studies was determined using Graphpad Prism software to calculate two-tailed unpaired *t* test or one-way or two-way ANOVA as appropriate. Significance thresholds were adjusted using Bonferroni correction to reduce type 1 errors.

GSE138696 Analysis. Microarray data (GSE138696 database) from peripheral blood mononuclear cells (PBMCs) collected from 16 AML patients (8 with monosomal karyotype [MK] and TP53 mutations and 8 normal karyotype with WT TP53 treated with DAC (20 mg/m2 intravenously over 1 h for 5 d) on the DECIDER trial (NCT00867672).

Data Availability. Raw and processed data files related to gene expression microarray are available through the Gene Expression Omnibus (GEO) database repository under accession GSE197405.

ACKNOWLEDGMENTS. Our studies were supported by funding from the Leukemia Lymphoma Society (A.A.K., M.R.B., and F.V.R.); the Adelson Medical Research Foundation (L.J.M., M.J.T., F.V.R., and S.B.B.); National Cancer Institute (NCI)–Cancer Center Support Grant P30 CA134274, the University of Maryland Marlene and Stewart Greenebaum Comprehensive Cancer Center Cigarette Restitution Funds (F.V.R.); the Molecular Medicine Graduate Program, University of Maryland (A.A.K., L.J.M., L.S., and T.M.C.); the Maryland Department of Health's Cigarette Restitution Fund Program (F.V.R., M.R.B., and A.A.K.); and the Van Andel Research Institute's Stand Up to Cancer Epigenetics Dream Team (S.B.B., F.V.R., and A.A.K.). Stand Up to Cancer is a program of the Entertainment Industry Foundation, administered by the American Association for Cancer Research. M.J.T. is a recipient of the Evelyn Grollman Glick Scholar Award. The Specialized Program of Research Excellence program, through NCI grant P50CA254897 supports F.R., S.B.B., M.J.T., A.J.D., and L.S. The content is solely the responsibility of the authors and does not necessarily represent the official views of the NIH, the Department of Health and Human Services, or the US government. We thank Nicole Glynn-Cunningham, MS, University of Maryland Greenebaum Comprehensive Cancer Center for procuring AML patient samples. We thank Feng Zhang, PhD, for gifting the lentiCRISPR v2 plasmid (Addgene plasmid No. 52961; http://n2t.net/addgene:52961; RRID:Addgene_52961).

Author affiliations: [a]Marlene and Stewart Greenebaum Comprehensive Cancer Center, University of Maryland School of Medicine, Baltimore, MD 21201; [b]Department of Radiation Oncology, University of Maryland School of Medicine, Baltimore, MD 21201; [c]Department of Oncology, Sidney Kimmel Comprehensive Cancer Center at Johns Hopkins, Baltimore, MD 21231; [d]Center for Stem Cell Biology and Regenerative Medicine, University of Maryland School of Medicine, Baltimore, MD 21201; [e]Department of Physiology, University of Maryland School of Medicine, Baltimore, MD 21201; [f]Department of Medicine, University of Maryland School of Medicine, Baltimore, MD 21201; and [g]Van Andel Research Institute, Grand Rapids, MI 49503

1. E. Conway O'Brien, S. Prideaux, T. Chevassut, The epigenetic landscape of acute myeloid leukemia. *Adv. Hematol.* **2014**, 103175 (2014).
2. A. A. Kogan, R. G. Lapidus, M. R. Baer, F. V. Rassool, Exploiting epigenetically mediated changes: Acute myeloid leukemia, leukemia stem cells and the bone marrow microenvironment. *Adv. Cancer Res.* **141**, 213–253 (2019).
3. L. Bullinger, K. Döhner, H. Döhner, Genomics of acute myeloid leukemia diagnosis and pathways. *J. Clin. Oncol.* **35**, 934–946 (2017).
4. D. Bowen *et al.*, TP53 gene mutation is frequent in patients with acute myeloid leukemia and complex karyotype, and is associated with very poor prognosis. *Leukemia* **23**, 203–206 (2009).
5. C. Haferlach *et al.*, Mutations of the TP53 gene in acute myeloid leukemia are strongly associated with a complex aberrant karyotype. *Leukemia* **22**, 1539–1541 (2008).
6. F. G. Rücker *et al.*, TP53 alterations in acute myeloid leukemia with complex karyotype correlate with specific copy number alterations, monosomal karyotype, and dismal outcome. *Blood* **119**, 2114–2121 (2012).
7. B. Tiwari, A. E. Jones, J. M. Abrams, Transposons, p53 and genome security. *Trends Genet.* **34**, 846–855 (2018).
8. R. M. Hoffman, Is DNA methylation the new guardian of the genome? *Mol. Cytogenet.* **10**, 11, 1–7 (2017).
9. J. P. Issa *et al.*, Phase 1 study of low-dose prolonged exposure schedules of the hypomethylating agent 5-aza-2′-deoxycytidine (decitabine) in hematopoietic malignancies. *Blood* **103**, 1635–1640 (2004).
10. H. Kantarjian *et al.*, Results of a randomized study of 3 schedules of low-dose decitabine in higher-risk myelodysplastic syndrome and chronic myelomonocytic leukemia. *Blood* **109**, 52–57 (2007).
11. J. P. Issa, DNA methylation as a therapeutic target in cancer. *Clin. Cancer Res.* **13**, 1634–1637 (2007).

12. S. B. Baylin, P. A. Jones, A decade of exploring the cancer epigenome - biological and translational implications. *Nat. Rev. Cancer* **11**, 726–734 (2011).
13. K. A. Fennell, C. C. Bell, M. A. Dawson, Epigenetic therapies in acute myeloid leukemia: where to from here? *Blood* **134**, 1891–1901 (2019).
14. M. Nieto *et al.*, The absence of p53 is critical for the induction of apoptosis by 5-aza-2′-deoxycytidine. *Oncogene* **23**, 735–743 (2004).
15. L. Yi, Y. Sun, A. Levine, Selected drugs that inhibit DNA methylation can preferentially kill p53 deficient cells. *Oncotarget* **5**, 8924–8936 (2014).
16. J. S. Welch *et al.*, TP53 and decitabine in acute myeloid leukemia and myelodysplastic syndromes. *N. Engl. J. Med.* **375**, 2023–2036 (2016).
17. H. Döhner *et al.*, Cytogenetics and gene mutations influence survival in older patients with acute myeloid leukemia treated with azacitidine or conventional care. *Leukemia* **32**, 2546–2557 (2018).
18. P. Bories *et al.*, Impact of TP53 mutations in acute myeloid leukemia patients treated with azacitidine. *PLoS One* **15**, e0238795 (2020).
19. H. C. Tsai *et al.*, Transient low doses of DNA-demethylating agents exert durable antitumor effects on hematological and epithelial tumor cells. *Cancer Cell* **21**, 430–446 (2012).
20. N. E. Muvarak *et al.*, Enhancing the cytotoxic effects of PARP inhibitors with DNA demethylating agents - A potential therapy for cancer. *Cancer Cell* **30**, 637–650 (2016).
21. I. Faraoni, G. Graziani, Role of BRCA mutations in cancer treatment with Poly(ADP-ribose) polymerase (PARP) inhibitors. *Cancers (Basel)* **10**, 487 (2018).
22. H. E. Bryant *et al.*, Specific killing of BRCA2-deficient tumours with inhibitors of poly(ADP-ribose) polymerase. *Nature* **434**, 913–917 (2005).
23. T. Helleday, The underlying mechanism for the PARP and BRCA synthetic lethality: clearing up the misunderstandings. *Mol. Oncol.* **5**, 387–393 (2011).
24. J. Murai *et al.*, Trapping of PARP1 and PARP2 by clinical PARP inhibitors. *Cancer Res.* **72**, 5588–5599 (2012).
25. R. Abbotts *et al.*, DNA methyltransferase inhibitors induce a BRCAness phenotype that sensitizes NSCLC to PARP inhibitor and ionizing radiation. *Proc. Natl. Acad. Sci. U.S.A.* **116**, 22609–22618. (2019).
26. J. Mateo *et al.*, DNA-repair defects and olaparib in metastatic prostate cancer. *N. Engl. J. Med.* **373**, 1697–1708 (2015).
27. A. D. D'Andrea, Susceptibility pathways in Fanconi's anemia and breast cancer. *N. Engl. J. Med.* **362**, 1909–1919 (2010).
28. L. J. McLaughlin *et al.*, Pharmacologic induction of innate immune signaling directly drives homologous recombination deficiency. *Proc. Natl. Acad. Sci. U.S.A.* **117**, 17785–17795 (2020).
29. T. S. Weiser *et al.*, Sequential 5-Aza-2 deoxycytidine-depsipeptide FR901228 treatment induces apoptosis preferentially in cancer cells and facilitates their recognition by cytolytic T lymphocytes specific for NY-ESO-1. *J. Immunother.* **24**, 151–161 (2001).
30. S. Oi *et al.*, Synergistic induction of NY-ESO-1 antigen expression by a novel histone deacetylase inhibitor, valproic acid, with 5-aza-2′-deoxycytidine in glioma cells. *J. Neurooncol.* **92**, 15–22 (2009).
31. A. Moreno-Bost *et al.*, Epigenetic modulation of MAGE-A3 antigen expression in multiple myeloma following treatment with the demethylation agent 5-azacitidine and the histone deacetlyase inhibitor MGCD0103. *Cytotherapy* **13**, 618–628 (2011).
32. K. B. Chiappinelli *et al.*, Inhibiting DNA methylation causes an interferon response in cancer via dsRNA including endogenous retroviruses. *Cell* **162**, 974–986 (2015).
33. H. Li *et al.*, Immune regulation by low doses of the DNA methyltransferase inhibitor 5-azacitidine in common human epithelial cancers. *Oncotarget* **5**, 587–598 (2014).
34. J. Wrangle *et al.*, Alterations of immune response of Non-Small Cell Lung Cancer with Azacytidine. *Oncotarget* **4**, 2067–2079 (2013).
35. V. Alcazer, P. Bonaventura, S. Depil, Human endogenous retroviruses (HERVs): Shaping the innate immune response in cancers. *Cancers (Basel)* **12**, 610 (2020).
36. L. Deng *et al.*, STING-dependent cytosolic DNA sensing promotes radiation-induced type I interferon-dependent antitumor immunity in immunogenic tumors. *Immunity* **41**, 843–852 (2014).
37. L. Ding *et al.*, PARP inhibition elicits STING-dependent antitumor immunity in Brca1-deficient ovarian cancer. *Cell Rep.* **25**, 2972–2980.e5 (2018).
38. S. R. Paludan, L. S. Reinert, V. Hornung, DNA-stimulated cell death: implications for host defence, inflammatory diseases and cancer. *Nat. Rev. Immunol.* **19**, 141–153 (2019).
39. A. J. Levine, S. L. Berger, The interplay between epigenetic changes and the p53 protein in stem cells. *Genes Dev.* **31**, 1195–1201 (2017).
40. K. I. Leonova *et al.*, p53 cooperates with DNA methylation and a suicidal interferon response to maintain epigenetic silencing of repeats and noncoding RNAs. *Proc. Natl. Acad. Sci. U.S.A.* **110**, E89–E98 (2013).
41. J. Kwon, S. F. Bakhoum, The cytosolic DNA-sensing cGAS-STING pathway in cancer. *Cancer Discov.* **10**, 26–39 (2020).
42. C. Kim, X. D. Wang, Y. Yu, PARP1 inhibitors trigger innate immunity via PARP1 trapping-induced DNA damage response. *eLife* **9**, e60637 (2020).
43. M. J. Topper *et al.*, Epigenetic therapy ties MYC depletion to reversing immune evasion and treating lung cancer. *Cell* **171**, 1284–1300.e21 (2017).
44. G. Greve *et al.*, Decitabine induces gene derepression on monosomic chromosomes: *In vitro* and *in vivo* effects in adverse-risk cytogenetics AML. *Cancer Res.* **81**, 834–846 (2021).
45. K. D. Sullivan, M. D. Galbraith, Z. Andrysik, J. M. Espinosa, Mechanisms of transcriptional regulation by p53. *Cell Death Differ.* **25**, 133–143 (2018).
46. P. G. Komarov *et al.*, A chemical inhibitor of p53 that protects mice from the side effects of cancer therapy. *Science* **285**, 1733–1737 (1999).
47. The Cancer Genome Atlas Research Network *et al.*, The Cancer Genome Atlas Pan-Cancer analysis project. *Nat Genet* **45**, 1113–1120 (2013).
48. D. Szklarczyk *et al.*, STRING v11: Protein-protein association networks with increased coverage, supporting functional discovery in genome-wide experimental datasets. *Nucleic Acids Res.* **47** (D1), D607–D613 (2019).
49. D. M. Schwartz *et al.*, JAK inhibition as a therapeutic strategy for immune and inflammatory diseases. *Nat. Rev. Drug Discov.* **17**, 78, 843–862 (2017).
50. S. M. Haag *et al.*, Targeting STING with covalent small-molecule inhibitors. *Nature* **559**, 269–273 (2018).
51. A. Mopin, V. Driss, C. Brinster, A detailed protocol for characterizing the murine C1498 cell line and its associated leukemia mouse model. *J. Vis. Exp.* (116): 10.3791/54270. (2016).
52. L. A. Donehower *et al.*, Mice deficient for p53 are developmentally normal but susceptible to spontaneous tumours. *Nature* **356**, 215–221 (1992).
53. M. L. Stone *et al.*, Epigenetic therapy activates type I interferon signaling in murine ovarian cancer to reduce immunosuppression and tumor burden. *Proc. Natl. Acad. Sci. U.S.A.* **114**, E10981–E10990 (2017).
54. C. S. Heiko Becker *et al.*, Randomized phase II study of all-trans retinoic acid and valproic acid added to decitabine in newly diagnosed elderly AML patients (DECIDER trial): Predictive impact of TP53 status. *Blood* **138**, ●●● (2021).
55. J. Ahn, G. N. Barber, STING signaling and host defense against microbial infection. *Exp. Mol. Med.* **51**, 1–10 (2019).
56. M. A. Sammons, T. T. Nguyen, S. S. McDade, M. Fischer, Tumor suppressor p53: from engaging DNA to target gene regulation. *Nucleic Acids Res.* **48**, 8848–8869 (2020).
57. F. Bao, P. R. LoVerso, J. N. Fisk, V. B. Zhurkin, F. Cui, p53 binding sites in normal and cancer cells are characterized by distinct chromatin context. *Cell Cycle* **16**, 2073–2085 (2017).
58. C. R. Harris *et al.*, p53 responsive elements in human retrotransposons. *Oncogene* **28**, 3857–3865 (2009).
59. K. Kim *et al.*, Outcomes of TP53-mutant acute myeloid leukemia with decitabine and venetoclax. *Cancer* **127**, 3772–3781 (2021).
60. G. E. Konecny, R. S. Kristeleit, PARP inhibitors for BRCA1/2-mutated and sporadic ovarian cancer: current practice and future directions. *Br. J. Cancer* **115**, 1157–1173 (2016).
61. J. Shen *et al.*, PARPi triggers the STING-dependent immune response and enhances the therapeutic efficacy of immune checkpoint blockade independent of BRCAness. *Cancer Res.* **79**, 311–319 (2019).
62. N. Muvarak *et al.*, c-MYC generates repair errors via increased transcription of alternative-NHEJ factors, LIG3 and PARP1, in tyrosine kinase-activated leukemias. *Mol. Cancer Res.* **13**, 699–712 (2015).
63. L. A. Tobin *et al.*, Targeting abnormal DNA repair in therapy-resistant breast cancers. *Mol. Cancer Res.* **10**, 96–107 (2012).
64. A. Ray Chaudhuri, A. Nussenzweig, The multifaceted roles of PARP1 in DNA repair and chromatin remodelling. *Nat. Rev. Mol. Cell Biol.* **18**, 610–621 (2017).
65. M. M. Rosado, E. Bennici, F. Novelli, C. Pioli, Beyond DNA repair, the immunological role of PARP-1 and its siblings. *Immunology* **139**, 428–437 (2013).
66. B. A. Flood, E. F. Higgs, S. Li, J. J. Luke, T. F. Gajewski, STING pathway agonism as a cancer therapeutic. *Immunol. Rev.* **290**, 24–38 (2019).
67. O. Sokolowska, D. Nowis, STING signaling in cancer cells: Important or not? *Arch. Immunol. Ther. Exp. (Warsz.)* **66**, 125–132 (2018).
68. J. Wayne, T. Brooks, A. Landras, A. J. Massey, Targeting DNA damage response pathways to activate the STING innate immune signaling pathway in human cancer cells. *FEBS J.* **288**, 4507–4540. (2021).
69. E. E. Parkes *et al.*, Activation of STING-dependent innate immune signaling by S-phase-specific DNA damage in breast cancer. *J. Natl. Cancer Inst.* **109**, ●●● (2016).
70. G. Dunphy *et al.*, Non-canonical activation of the DNA sensing adaptor STING by ATM and IFI16 mediates NF-κB signaling after nuclear DNA damage. *Mol. Cell* **71**, 745–760.e5 (2018).
71. D. Liao, M. Wang, Y. Liao, J. Li, T. Niu, A review of efficacy and safety of checkpoint inhibitor for the treatment of acute myeloid leukemia. *Front. Pharmacol.* **10**, 609, 1–11(2019).
72. J. Vadakekolathu *et al.*, Immune landscapes predict chemotherapy resistance and immunotherapy response in acute myeloid leukemia. *Sci. Transl. Med.* **12**, 546 (2020).
73. A. Chatterjee *et al.*, Marked global DNA hypomethylation is associated with constitutive PD-L1 expression in melanoma. *iScience* **4**, 312–325 (2018).
74. A. A. Emran *et al.*, Targeting DNA methylation and EZH2 activity to overcome melanoma resistance to immunotherapy. *Trends Immunol.* **40**, 328–344 (2019).
75. A. Perrier, A. Didelot, P. Laurent-Puig, H. Blons, S. Garinet, Epigenetic mechanisms of resistance to immune checkpoint inhibitors. *Biomolecules* **10**, ●●● (2020).
76. M. Wang, Y. Liu, Y. Cheng, Y. Wei, X. Wei, Immune checkpoint blockade and its combination therapy with small-molecule inhibitors for cancer treatment. *Biochim. Biophys. Acta Rev. Cancer* **1871**, 199–224 (2019).
77. L. Wang *et al.*, Decitabine enhances lymphocyte migration and function and synergizes with CTLA-4 blockade in a murine ovarian cancer model. *Cancer Immunol. Res.* **3**, 1030–1041 (2015).
78. H. Liu, Emerging agents and regimens for AML. *J. Hematol. Oncol.* **14**, 49 (2021).
79. A. Colaprico *et al.*, TCGAbiolinks: an R/Bioconductor package for integrative analysis of TCGA data. *Nucleic Acids Res.* **44**, e71 (2016).
80. J. Vadakekolathu *et al.*, TP53 abnormalities correlate with immune infiltration and associate with response to flotetuzumab immunotherapy in AML. *Blood Adv.* **4**, 5011–5024 (2020).
81. G. Korotkevich *et al.* , Fast gene set enrichment analysis. bioRxiv [preprint](2021). https://www.biorxiv.org/content/10.1101/060012v3. Accessed 20 June 2022.
82. A. Subramanian *et al.*, Gene set enrichment analysis: a knowledge-based approach for interpreting genome-wide expression profiles. *Proc. Natl. Acad. Sci. U.S.A.* **102**, 15545–15550 (2005).
83. R. Kolde, Pheatmap: pretty heatmaps. *R package version* **1** (2012).
84. C. von Mering *et al.*, STRING: known and predicted protein-protein associations, integrated and transferred across organisms. *Nucleic Acids Res.* **33**, D433–D437 (2005).